THE JOURNAL OF PHYSICAL CHEMISTRY B

ARTICLE

pubs.acs.org/JPCB

Molecular Dynamics Simulation of Tri-*n*-butyl-Phosphate Liquid: A Force Field Comparative Study

Shengting Cui,*[,†] Valmor F. de Almeida,*[,‡] Benjamin P. Hay,[‡] Xianggui Ye,[†] and Bamin Khomami[†]

[†]Materials Research and Innovation Laboratory, Department of Chemical and Biomolecular Engineering, University of Tennessee, Knoxville, Tennessee 37996, United States

[‡]Oak Ridge National Laboratory, Oak Ridge, Tennessee 37831-6181, United States

Supporting Information

ABSTRACT: Molecular dynamics (MD) simulations were conducted to compare the performance of four force fields in predicting thermophysical properties of tri-*n*-butyl-phosphate (TBP) in the liquid phase. The intramolecular force parameters used were from the Assisted Model Building with Energy Refinement (AMBER) force field model. The van der Waals parameters were based on either the AMBER or the Optimized Potential for Liquid Simulation (OPLS) force fields. The atomic partial charges were either assigned by performing quantum chemistry calculations or utilized previously published data, and were scaled to approximate the average experimental value of the electric dipole moment. Canonical ensemble computations based on the aforementioned parameters were performed near atmospheric pressure and temperature to obtain the electric dipole moment, mass density, and self-diffusion coefficient. In addition, the microscopic structure of the liquid was characterized via pair correlation functions between selected atoms. It has been demonstrated that the electric dipole moment can be approximated within 1% of the average experimental value by virtue of scaled atomic partial charges. The liquid mass density can be predicted within 0.5−1% of its experimentally determined value when using the corresponding charge scaling. However, in all cases, the predicted self-diffusion coefficient is significantly smaller than a commonly quoted experimental measurement; this result is qualified by the fact that the uncertainty of the experimental value was not available.

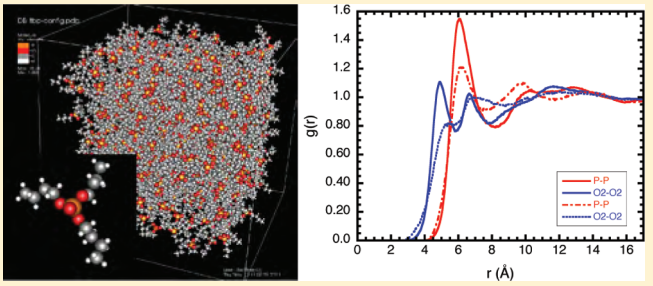

1. INTRODUCTION

In applications of liquid−liquid extraction processes for recycling of used nuclear fuel, the aqueous phase coexists with an organic extracting phase which consists of a mixture of an extracting agent and a diluent. A commonly used agent is the tri-*n*-butyl-phosphate (TBP) molecule which has been used to extract uranium,[1−4] plutonium,[5,6] zirconium,[7] and other metal cations.[8] With the current renewed interest in nuclear energy and waste management, there is interest in better understanding the molecular processes of extraction and determining the thermophysical properties of the phases involved.[9−12] However, to date, a systematic study of force field parameters for TBP in the liquid phase is still lacking.

Many experimental measurements of fundamental properties of TBP and related systems in the liquid phase were carried out in the early years of nuclear energy applications.[13] Nevertheless, some reported measurements still present significant variability, limited range, and/or lack of associated uncertainty, e.g., self-diffusivity and electric dipole moment. A recent experimental study[14] systematically measured the mass density and dynamics viscosity of TBP in the bulk phase and its mixture with dodecane at various mole fractions, thus providing a reference for calibration of molecular models.

Molecular modeling studies in recent years have investigated the fundamental molecular level behavior for some extraction systems. Wipff and co-workers have carried out MD simulation studies of systems involving TBP, such as TBP in vacuum and in chloroform,[15] the stoichiometry of TBP complexation in aqueous solution,[16] and TBP complexation with uranyl nitrate and acid dissolution in supercritical CO_2.[17]

We have also conducted a series of MD simulations which began to elucidate the processes of complex formation in the aqueous phase, migration to the interface and the effect of the interface in facilitating the formation of various complex species, and the detailed process of neutral species migration into the organic phase.[9−12] In these studies, to facilitate computational efficiency, we used united atom models for dodecane and the butyl tails of the TBP molecules. Although this approach is generally acceptable for providing a fundamental understanding and insight, in practical applications, it is necessary to employ all-atom models.

In this work, we report a characterization study of TBP bulk liquid behavior using all-atom models. Specifically, we have

Received: July 25, 2011
Revised: November 11, 2011
Published: November 29, 2011

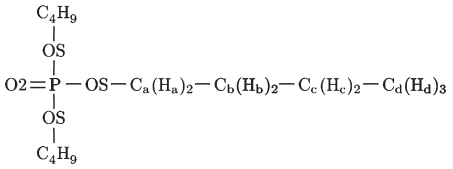

Figure 1. Schematic of a TBP molecule and its atom types. The bonded potential parameters for all carbon atoms were obtained from the AMBER CT type, and for hydrogen atoms, from either AMBER H1 or HC types (Tables 1−3). The nonbonded potential parameters for all atom types are presented in Table 4.

Table 1. AMBER Bond Length Stretch Energy and Length Parameters

bond type	K_r (kcal mol^{-1} Å^{-2})	r_{eq} (Å)
OS−P	230	1.610
OS−CT	320	1.410
P−O2	525	1.480
CT−H1	340	1.090
CT−HC	340	1.090
CT−CT	310	1.526

computed various properties of TBP in the liquid phase, namely, the mass density, self-diffusion coefficient, electric dipole moment, and microscopic structure as characterized by the pair correlation functions between heavy atoms. These computations have been carried out with different sets of van der Waals and atomic charge parameters to compare their predictive capability of thermophysical properties of TBP. In the following, we first describe the force field models and methods (section 2). In turn, results are discussed in section 3, and a summary of our findings is provided in section 4.

2. MODELS AND METHODS

The AMBER99[18] intramolecular parameter set for bond length stretching, bond angle bending, and dihedral angle torsion[19,20] was used in this work. The total interaction potential energy is in the form

$$E := \sum_{\text{bonds}} K_r(r - r_{eq})^2 + \sum_{\text{angles}} K_\theta(\theta - \theta_{eq})^2 + \sum_{\text{dihedrals}} \sum_n V_n(1 + \cos(n\phi - \gamma_n)) + \sum_{a<b} \left[\varepsilon_{ab} \left(\frac{R^*_{ab}}{r_{ab}} \right)^{12} - 2\varepsilon_{ab} \left(\frac{R^*_{ab}}{r_{ab}} \right)^{6} + \frac{C q_a q_b}{r_{ab}} \right] \quad (1)$$

The terms of (1) in order of appearance are the bond length stretching, bond angle bending, bond torsion, van der Waals, and electrostatic interactions, respectively, between atoms a and b. The parameters for the interaction potential of all atoms of a TBP molecule (Figure 1) are given in Tables 1−4. For the van der Waals and Coulomb interactions between 1−4 atoms in the same molecule, the AMBER convention was followed using reduction parameters of 1/2 and 1/1.2, respectively.[20]

For the Lennard-Jones (LJ) potential, we tested two sets of Lennard-Jones parameters: one is the original AMBER parameters, which we designate as AMBER; the other is the OPLS parameter set for the butyl tails of the TBP molecule, and it is thus designated as OPLS. Therefore, the LJ parameters for the phosphoryl group (i.e., the atoms P, O2, and OS in Figure 1) are the same for both AMBER and OPLS sets (Table 4).

Table 2. AMBER Bond Angle Bending Energy and Angle Parameters

angle type	K_q (kcal mol^{-1} rad^{-2})	θ_{eq} (deg)
CT−OS−P	100.0	120.5
OS−P−O2	100.0	108.23
OS−P−OS	45.0	102.6
OS−CT−H1	50.0	109.5
OS−CT−CT	50.0	109.5
H1−CT−HC	35.0	109.5
HC−CT−HC	35.0	109.5
CT−CT−H1	50.0	109.5
CT−CT−HC	50.0	109.5
CT−CT−CT	40.0	109.5

Table 3. AMBER Dihedral Torsion Energy and Angle Parameters

	V_n (kcal mol^{-1}), γ_n (deg)					
	n = 1		n = 2		n = 3	
dihedral type						
CT−OS−P−O2	0	0	0	0	0.25	0
CT−OS−P−OS	0	0	1.2	0	0.25	0
H1−CT−OS−P	0	0	0	0	0.383	0
CT−CT−OS−P	0	0	0	0	0.383	0
OS−CT−CT−HC	0.25	0	0	0	0.156	0
OS−CT−CT−CT	0	0	0	0	0.156	0
HC[a]−CT−CT−HC	0	0	0	0	0.15	0
CT−CT−CT−HC[b]	0	0	0	0	0.16	0
CT−CT−CT−CT	0.2	180	0.25	180	0.18	0

[a] Used in lieu of H1−CT−CT−HC which calls for γ_3 = 0.156. [b] Used in lieu of CT−CT−CT−H1 which calls for γ_3 = 0.156.

For the partial electric charges of the atoms in the TBP molecule, we tested the set developed by ref 15, which was obtained from an MNDO (Modified Neglect of Differential Overlap) semiempirical quantum chemistry calculation[21] which we designate as the MNDO charge. Another set tested was obtained from an *ab initio* Density Functional Theory (DFT) calculation we performed with atomic charges derived using the Restrained Electrostatic Potential charge fitting method,[22] which we designate as the DFT charge. We performed additional calculations by rescaling the original charges to approximate the average experimentally measured electric dipole moment.

The combination of the two sets of LJ parameters and the two sets of charges results in four sets of force field parameters, which we designate as

- AMBER-MNDO: AMBER LJ parameters with charges from MNDO
- AMBER-DFT: AMBER LJ parameters with charges from DFT
- OPLS-MNDO: OPLS LJ parameters for the butyl chains, AMBER LJ parameters for the phosphoryl group, with charges from DFT
- OPLS-DFT: OPLS LJ parameters for the butyl chains, AMBER LJ parameters for the phosphoryl group, with

Table 4. Lennard-Jones and Electric Charge Parameters[a]

	AMBER[18]		OPLS[28]		MNDO	DFT
atom type	ε_a[b]	σ_a[c]	ε_a[b]	σ_a[c]	q_a[d]	q_a[d]
O2	0.21	2.96	0.21	2.96	−0.87	−0.8083
P	0.20	3.742	0.20	3.742	1.77	1.6096
OS	0.17	3.0	0.17	3.0	−0.56	−0.6158
C_a	0.1094	3.4	0.066	3.5	0.2	0.3637
C_b	0.1094	3.4	0.066	3.5	0.06	0.0260
C_c	0.1094	3.4	0.066	3.5	0.02	0.1213
C_d	0.1094	3.4	0.066	3.5	0.02	−0.0326
H_a	0.0157	2.65	0.03	2.5	−0.02	−0.0261
H_b	0.0157	2.65	0.03	2.5	0	0.0007
H_c	0.0157	2.65	0.03	2.5	0	−0.0387
H_d	0.0157	2.65	0.03	2.5	0	−0.0005

[a] The van der Waals parameters in (1) are related to the commonly used Lennard-Jones parameters in the form $4\varepsilon_{ab}[(\sigma_{ab}/r_{ab})^{12} - (\sigma_{ab}/r_{ab})^{6}]$, with $\sigma_{ab} = R^*_{ab}/2^{1/6}$, while ε_{ab} remains unchanged. The following AMBER combining rules are used for interactions between dissimilar atoms: $\varepsilon_{ab} = (\varepsilon_a\varepsilon_b)^{1/2}$ and $\sigma_{ab} = (1/2)(\sigma_a + \sigma_b)$. Non-bonded interaction potentials for intramolecular 1−4 atoms are applied with scaling factors 1/2 and 1/1.2 for van der Walls and electrostatics, respectively. All hydrogen atoms have the same van der Waals parameters within each set. For the AMBER LJ parameters, all hydrogen atoms were considered as HC type following ref 15; similarly for OPLS, i.e., H-alkane type. [b] In kcal mol^{-1}. [c] In Å. [d] In e.

charges from DFT. As stated earlier, the intramolecular parameters for all the above-mentioned combinations are the same and derived from AMBER (Tables 1−3).

The DFT charges were determined by performing an *ab initio* quantum chemistry calculation in which the structure of the TBP molecule was optimized using DFT with the B3LYP/TZVP basis set.[23−25] The DFT charges were obtained through fitting to this geometry using the RHF/6-31+G* level of theory. On the basis of symmetry, the equivalent carbons (i.e., at the same position relative to the P atom in the molecule) and hydrogen atoms on the three butyl tails were restricted to have the same atomic charges.

The long-range electrostatic interaction is treated via Ewald sums[26,27]

$$\begin{aligned} U :=& \frac{1}{2}\sum_i\sum_a q_{ia}\sum_{j\neq i}\sum_b q_{jb}\,\mathrm{erfc}(\kappa r_{iajb})/r_{iajb} \\ &+\frac{1}{2}\sum_i\sum_a q_{ia}\sum_b{}' q_{jb}\,\mathrm{erfc}(\kappa r_{iajb})/r_{iajb} \\ &+\frac{2\pi}{V}\sum_{\mathbf{h}\neq\mathbf{0}} Q(h)S(\mathbf{h})S(-\mathbf{h}) - \frac{\kappa}{\sqrt{\pi}}\sum_i\sum_a {q_{ia}}^2 \\ &-\frac{1}{2}\sum_i\sum_a\sum_b{}'' \chi_{ab}q_{ia}q_{ib}\,\mathrm{erf}(\kappa r_{iaib})/r_{iaib} \end{aligned} \tag{2}$$

where i and j represent two distinct molecules and a and b, two distinct atoms. The prime in the summation in the second term indicates that only those atoms separated by three or more bonds are included. The double prime in the last term means that the summation includes only the atom pairs connected by a bond stretching, a bond bending, and a dihedral angle. Care was taken in the subtraction of the atom pair connected by the torsional bond to properly account for the reduction of the electrostatic interaction by the factor 1/1.2. To that end, χ_{ab}, in (2), was used to account for this reduction as follows. For two atoms connected by bond stretching and bond angle bending, $\chi_{ab} = 1$. For two atoms connected by bond torsion (i.e., 1−4 atom pairs), $\chi_{ab} = 1/6$.

The factors $Q(h)$ and $S(\mathbf{h})$ are defined by

$$Q(h) := \frac{1}{h^2}\exp\left(\frac{-h^2}{4\kappa^2}\right) \tag{3}$$

$$S(\mathbf{h}) := \sum_i\sum_a q_{ia}\exp(i\mathbf{h}\cdot\mathbf{r}_{ia}) \tag{4}$$

with the Cartesian reciprocal lattice vector $\mathbf{h} := 2\pi[(l/L_x), (m/L_y), (n/L_z)]$, where $l, m, n = 0, \pm1, \pm2, \ldots, \pm\infty$, and $h := |\mathbf{h}|$.

An Ewald convergence factor $\kappa = 5/L$ was used for calculating the real space Ewald sums, where L is the box length in all three directions ($L_x = L_y = L_z = L$). All atoms in the primary simulation box are included in the summation. As the box length is relatively large, ≈60 Å, the real space summation is highly accurate. To speed up the calculations, a lookup table was used for the real space potential and force. In the reciprocal space, 15 k-space vectors in each direction were employed for the calculation of the interaction potential and force.

The calculation of the pressure in a canonical ensemble followed the method described in ref 29 wherein the molecular pressure tensor, $P^{(0)}_{\alpha\beta}$, including all but the electrostatic interaction is computed as

$$P^{(0)}_{\alpha\beta} := \frac{1}{V}\left[\sum_{i=1}^{N} m_i v_{i\alpha}v_{i\beta} + \sum_{i=1}^{N-1}\sum_{j>i}^{N}\sum_{a=1}^{n}\sum_{b=1}^{n}(\mathbf{r}_{ij})_\alpha(\mathbf{f}_{iajb})_\beta\right] \tag{5}$$

α and β are the indices of the Cartesian components of a vector or tensor. m_i and v_i are the mass and velocity of molecule i, respectively; $(\boldsymbol{r}_{ij})_\alpha$ is the α-component of the center-of-mass distance between molecules i and j; $(\mathbf{f}_{iajb})_\beta$ is the β-component of the force between atom a of molecule i and atom b of molecule j; and V is the volume of the system. The second term in (5) accounts for the virial contribution of the pressure tensor, excluding the electrostatic interaction.

When the Ewald summation method is used, (5) is not applicable because the contribution from the reciprocal space to the pressure tensor cannot be expressed in the virial form. In this case, an expression has been derived in ref 29 where the electrostatic contribution to the pressure tensor, $P^{(q)}_{\alpha\beta}$, is obtained from

$$\begin{aligned} VP^{(q)}_{\alpha\beta} =& \frac{1}{2}\sum_i\sum_a q_{ia}\sum_{j\neq i}\sum_b q_{jb}\left[\frac{2}{\sqrt{\pi}}\kappa r_{iajb}\exp(-\kappa^2 r^2_{iajb}) + \mathrm{erfc}(\kappa r_{iajb})\right] \\ &\times\frac{(r_{ij})_\alpha(r_{iajb})_\beta}{{r_{iajb}}^3} + \frac{2\pi}{V}\sum_{\mathbf{h}\neq0}Q(h)S(\mathbf{h})S(-h)\left(\delta_{\alpha\beta} - \frac{2h_\alpha h_\beta}{h^2} - \frac{h_\alpha h_\beta}{2\kappa^2}\right) \\ &-\frac{2\pi}{V}\sum_i\sum_a q_{ia}(\mathbf{p}_{ia})_\beta\sum_{\mathbf{h}\neq0}Q(h)ih_\alpha[S(\mathbf{h})\exp(-i\mathbf{h}\cdot\mathbf{r}_{ia}) \\ &-S(-\mathbf{h})\exp(i\mathbf{h}\cdot\mathbf{r}_{ia})] \end{aligned} \tag{6}$$

Here, $r := |\mathbf{r}|$, $\delta_{\alpha\beta}$ is the Kronecker delta, $\mathbf{p}_{ia} := \mathbf{r}_{ia} - \mathbf{r}_i$ is a vector between atom a and the center of mass of molecule i, and $\mathbf{r}_{iajb} := \mathbf{r}_{ia} - \mathbf{r}_{jb}$. The total pressure tensor is then $P_{\alpha\beta} := P^{(0)}_{\alpha\beta} + P^{(q)}_{\alpha\beta}$.

The calculations were performed using 500 TBP molecules at 25 °C. For the LJ interaction, a cutoff distance of 15 Å was used and the interaction potential shifted. Standard tail correction to the pressure is included for the LJ interaction.[27] The equations of

dx.doi.org/10.1021/jp207089e |J. Phys. Chem. B 2012, 116, 305–313

Table 5. Calculated Electric Dipole Moment of TBP in the Liquid Phase at the Experimental Mass Density of 0.9708 g cm^{-3} [14] under ambient conditions (25 °C, 1 bar)[a]

p_D (D)			
OPLS-MNDO	OPLS-DFT	AMBER-MNDO	AMBER-DFT
	$q = q_0$		
4.93 ± 0.14	3.80 ± 0.10	4.97 ± 0.11	3.91 ± 0.11
	$q = 0.8q_0$		
4.09 ± 0.06	3.31 ± 0.05	4.13 ± 0.05	3.34 ± 0.06
	$q = 0.7q_0$		
3.70 ± 0.04	2.99 ± 0.04	3.68 ± 0.06	–[c]
	$q = 0.6q_0$		
3.23 ± 0.04	–[b]	3.24 ± 0.03	–[c]

[a] Results are presented for all force fields as a function of charge scaling. q_0 represents the non-scaled charges in Table 4. The experimentally measured values of p_d are in the range 3.07−3.32 D.[33,34] [b] Not computed because expected to be lower than the experimental range. [c] Not computed because of poor self-diffusion.

motion were integrated using the reversible multiple time step method[30] with a time step of 1−1.5 to strictly conserve the total Hamiltonian of the system. In all computations, the systems were equilibrated for at least 30 ps using a velocity rescaling thermostat and another 30 ps, or longer, using the Nosé thermostat.[31,32] The pressure variation with time indicated that, at the end of the equilibration, the pressure had relaxed to the equilibrium. The equilibrium pressure was obtained from at least a 450 ps long calculation; some calculations were executed for as long as 1.5 ns.

3. RESULTS AND DISCUSSION

All simulations described henceforth were done with NVT ensembles at 25 °C. The mass density prediction at 1 bar was obtained by interpolating the values of the imposed mass density and calculated pressure for three realizations around the value of the experimentally measured mass density under ambient conditions.[14] This is possible because the pressure varies linearly with respect to a small variation of mass density.

The calculated values for the electric dipole moment and self-diffusion coefficients were not interpolated to ambient pressure. Instead, they were computed at the experimentally measured value for mass density at 25 °C and 1 bar. The calculation of these quantities at ambient pressure requires further work beyond the current scope. However, they are not expected to vary significantly.

3.1. Electric Dipole Moment. The electric dipole moment for TBP, p_D, in the liquid state was computed from

$$\mathbf{p}_i := \sum_a q_a(\mathbf{r}_{ia} - \mathbf{r}_i^{COM}) \quad \text{and}$$

$$p_D := \left\langle \left(\frac{1}{N} \sum_{i=1}^{N} p_i^2 \right)^{1/2} \right\rangle \tag{7}$$

where $\mathbf{p}_i$ is the instantaneous electric dipole moment vector of the ith molecule. The summation runs through all atoms a in a molecule. The ensemble average (7) of the magnitude of the dipole moment over all molecules in the system produces the dipole moment.

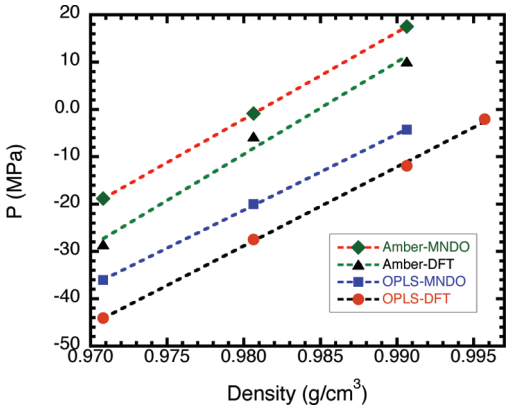

Figure 2. Pressure variation with mass density at 25 °C used for interpolating the mass density at ambient pressure, 0.1 MPa (Table 6).

To our knowledge, the experimental value of the dipole moment under ambient conditions varies in the range 3.07−3.32 D.[33,34] The calculated p_D values for all force field sets (Tables 1−4) are greater than this range (Table 5, results for $q = q_0$). The maximum dipole moment is predicted by the OPLS-MNDO parameter set, 4.93 ± 0.14 D, while the minimum is predicted by the OPLS-DFT force field, 3.80 ± 0.10 D. These higher values are consistent with other simulations which have reported p_D = 4.84 D.[16] In fact, the suggestion is made that, in dense liquids, TBP molecules prefer conformations that are more extended than that of isolated molecules in a vacuum.

Since TBP is a neutral, polar molecule, it is important to approximate the value of the experimental dipole moment because it is a quantity central to the extracting behavior of this agent. One approach in obtaining the effective atomic partial charges that approximate the experimental dipole moment is to carry out statistical averaging over all conformational states; this entails a high computational cost. Since most of the significant partial charges of the TBP molecules are located on or near the phosphoryl group, we have taken a simple approach here to rescale the original quantum-calculated charges and to carry out a series of calculations so that the model approximates the experimentally measured dipole moment.

When the MNDO charge is scaled by a factor of ≈0.60, the dipole moment reduces to ≈3.2 D, while, for the DFT charges scaled by ≈0.7, p_D ≈ 3.0 D. Since these rescaled charge sets approximate the dipole moment, they may be considered as effective charges that describe the electric interactions of TBP molecules in the liquid state. In subsequent sections, scaled and unscaled charges will be used for predicting the mass density and self-diffusion coefficient of TBP.

3.2. Mass Density. The calculation of the pressure, $P_{\alpha\beta}$, at several mass densities near the experimentally measured value of 0.9708 g cm^{-3} [14] allows for a linear interpolated (or extrapolated) value at 1 bar (Figure 2 and Supporting Information section 4). The mass density results for all force fields with unscaled charges (hence higher dipole moment, $q = q_0$ in Table 5) are consistently higher than the experimental value (Table 6). The relative deviations are 1.06% for AMBER-MNDO, 1.45% for AMBER-DFT, 2.32% for OPLS-MNDO, and 2.73% for OPLS-DFT.

The use of scaled partial atomic charges improved the prediction of mass density (Table 6). The corresponding relative deviation from the experimental value is 0.45% for AMBER-MNDO (underestimates the density), 0.47% for OPLS-MNDO

Table 6. Computed Mass Density at Ambient Pressure (1 bar) and 25 °C for all Force Fields including Charge Scaling (Experimental Value: 0.9708 g cm^{-3})[14]

mass density (g cm^{-3})			
OPLS-MNDO	OPLS-DFT	AMBER-MNDO	AMBER-DFT
unscaled charges			
0.9931	0.9978	0.9811	0.9837
scaled charges			
0.9754[a]	0.9803[b]	0.9664[a]	–[c]

[a] Scale factor: 0.6. [b] Scale factor: 0.7. [c] Not calculaed by virtue of poor self-diffusion.

(overestimates the density), and 0.98% for OPLS-DFT (overestimates the density). Scaled charge calculation for AMBER-DFT was not performed due to the low diffusion coefficient predicted by this force field set (section 3.3).

A couple of observations are in order when comparing the results obtained for the unscaled partial atomic charges against the corresponding scaled charges. First, the mass density is not greatly affected by relatively small changes in the partial atomic charges. This may be due to the weaker effect of dipole−dipole interaction compared to charge−charge interaction and a lack of hydrogen bonding structure, since the butyl tails are hydrophobic. Second, the model improvement in approximating the experimental value of the dipole moment resulted in a more accurate prediction of the mass density for all force fields.

3.3. Self-Diffusion Coefficient. The self-diffusion coefficient was calculated using the Einstein relation

$$\left\langle \frac{1}{N}\sum_{i=1}^{N} |\mathbf{r}_i^{\mathrm{COM}}(t) - \mathbf{r}_i^{\mathrm{COM}}(0)|^2 \right\rangle = 6Dt \qquad (8)$$

where $\mathbf{r}_i^{\mathrm{COM}}(t)$ is the center of mass of a TBP molecule i at time t, N is the number of molecules in the system, the angle bracket represents an ensemble average (an equivalent MD simulation time average), D is the diffusion coefficient, and t is the elapsed time.

Calculations of the diffusion coefficient were made at the mass density corresponding to the experimental value 0.9708 g cm^{-3} under ambient conditions (25 °C, 1 bar)[14] via constant NVT simulations. The diffusion coefficient was derived on the basis of runs of 0.75−1.2 ns after equilibration. The mean square displacement (MSD) was obtained from following the molecular trajectories in the MD simulation. A linear fit to the MSD using the Einstein relation 8 was performed to derive the self-diffusion coefficient.

The results obtained from the four types of force field models using unscaled and scaled partial atomic charges (Table 7) are considerably lower than the experimental value 2.29 × 10^{-6} cm^2 s^{-1} [35] commonly quoted under ambient conditions. When scaled charges are used, somewhat better agreement with the experimental value is obtained. The AMBER-DFT model produced a significantly lower value of the self-diffusion coefficient when using unscaled charges; hence, no further attempt was made to investigate whether scaled charges would be beneficial.

We also examined other factors that can affect the self-diffusion of TBP. One is the stiffness of the molecule which is partially affected by the scaling factor for the intramolecular van der Waals (Lennard-Jones) interaction. In the standard AMBER

Table 7. Calculated Self-Diffusion Coefficient of TBP in the Liquid Phase at the Experimental Mass Density of 0.9708 g cm^{-3} [14] under Ambient Conditions (25 °C, 1 bar)[a]

$D \times 10^7$ (cm^2 s^{-1})			
OPLS-MNDO	OPLS-DFT	AMBER-MNDO	AMBER-DFT
$q = q_0$			
4.15 ± 0.19	3.11 ± 0.3	3.17 ± 0.04	1.91 ± 0.23
$q = 0.7q_0$			
5.09 ± 0.24	4.99 ± 0.59	4.44 ± 0.5	–[c]
$q = 0.6q_0$			
5.37 ± 0.09	–[b]	4.07 ± 0.20	–[c]

[a] Results are presented for all force fields as a function of charge scaling. q_0 represents the unscaled charges in Table 4. The available, experimentally measured value of D is 2.29 × 10^{-6} cm^2 s^{-1}.[35] [b] Not computed because dipole moment expected to be out of experimental range. [c] Not computed because expected to be too low.

force field, a reduction factor of 0.5 is used for the 1−4 atoms connected by three atomic bonds. As noted in the original AMBER force field publication,[20] such a scaling factor is arbitrary. In fact, there is an indication[36] that a factor equal to 0.5 may be too large. Thus, we have carried out calculations with a van der Waals scaling factor of 0.1. Its use can increase the value of the self-diffusion coefficient by more than 50% compared with using a van der Waals scaling factor equal to 0.5. Thus, for the present models, the closest calculated self-diffusion coefficient to the experimentally reported value is 0.84 × 10^{-6} cm^2 s^{-1}, which is still about 2.7 times smaller than the experimental value.

The prediction of dynamical transport properties, such as the self-diffusion coefficient, in a first generation of force field models is usually less satisfactory than other thermodynamic properties. This is because the accurate prediction of transport properties requires models with improved molecular structure and molecular interaction fidelity. For the force fields used here, we have not optimized the van der Waals parameters for the phosphoryl group of the TBP molecule; they are taken directly from the AMBER parameter set which was originally optimized for biomolecules. Therefore, we speculate that fine-tuning the van der Waals parameters for the TBP headgroup could be beneficial for improving the prediction of the self-diffusion coefficient and possibly other transport properties.

3.4. Spatial Pair Correlation Functions (PCFs). The spatial pair correlation functions (PCF) between atoms of two interacting molecules can be used to gain insight into the microstructure of TBP in the liquid state. Also, such predictions can be verified via X-ray and/or neutron scattering. However, we are not aware of any available experimental results to date. An analysis of the PCFs is also useful from a theoretical perspective in providing insight for the understanding of macroscopic properties as well as how molecules interact in the liquid state bulk phase. A comparison of the pair correlation functions between the different force field models provides molecular scale characteristics complementary to experimental data.

Most of the discussion to follow involves the atoms on the phosphoryl group (those not discussed here are provided in the Supporting Information section 4). The differences between the pair correlation functions when using the AMBER and OPLS van der Waals force fields with the same set of partial atomic charges

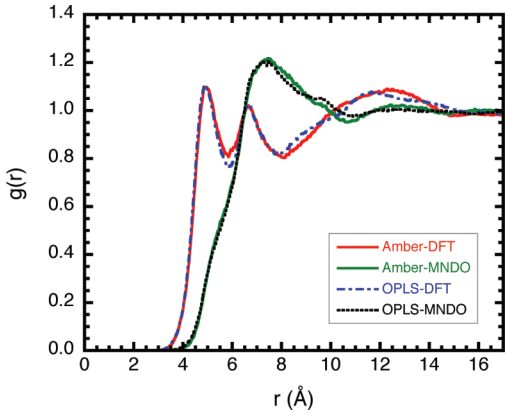

Figure 3. Intermolecular spatial pair correlation function between the pairs of atoms O2−O2 on two TBP molecules. Red solid line, AMBER-DFT; green solid line, AMBER-MNDO; blue long-dashed short-dashed line, OPLS-DFT; black dashed line, OPLS-MNDO.

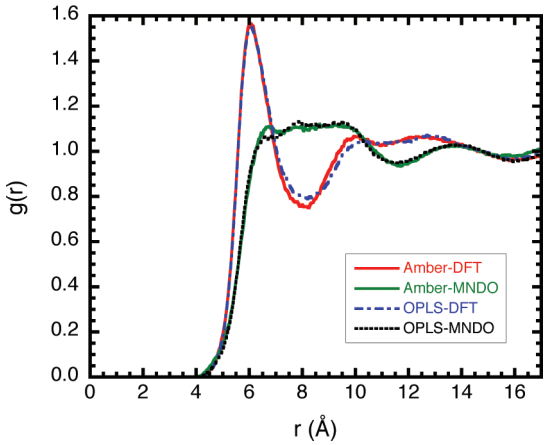

Figure 4. Pair correlation for P−P; line types as in Figure 3.

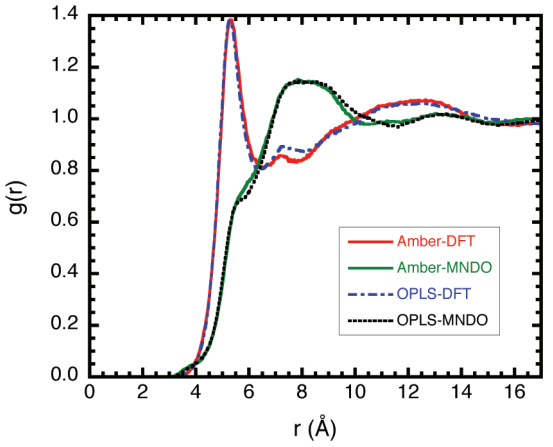

Figure 5. Pair correlation for P−O2; line types as in Figure 3.

are small; that is, the AMBER-DFT and OPLS-DFT produce virtually the same PCFs; the same is true for AMBER-MNDO and OPLS-MNDO. The reason for this similarity is that, as mentioned earlier, the LJ parameters are essentially the same for all models. The only difference is on the treatment of the van der Walls interaction for the butyl tails. Therefore, in the discussion that follows, results are presented on the basis of the charge set used, i.e., either DFT or MNDO.

3.4.1. O2−O2 Pair Correlation Function (Figure 3)

- DFT charge. There are two peaks located at the positions 4.9 and 6.7 Å, respectively, and a broad third peak at around 12 Å. The first peak position, 4.9 Å, is substantially larger than the close contact distance, ≈3.0 Å. Thus, the electrostatic repulsion between the O2 type atoms is an important factor in determining how the TBP molecules are packed in the liquid phase.
- MNDO charge. There is one peak at 7.5 Å with a weak shoulder starting around 9.0 Å. There also appears to be some weak deflection before reaching the first peak, suggesting possible shoulder-like behavior at shorter distances.

Comparison of the PCFs for the two sets of force field parameters suggests that the larger charges on the O2 and P atom types in the MNDO parameter set may have pushed the phosphoryl groups further apart than for the DFT charge set, resulting in the elimination of the first peak, while the main peak becomes higher.

3.4.2. P−P Pair Correlation Function (Figure 4)

- DFT charge. First peak around 6.2 Å with some weak structure between 10.0 and 13.5 Å.
- MNDO charge. The pair correlation function has a broad peak starting around 6.5 Å, running to about 10.0 Å. Beyond that, there is a weak peak at around 14 Å. The weaker repulsion for the DFT charge allows a closer approach between the phosphoryl groups of two TBP molecules, resulting in a well-defined peak. For the MNDO charge, the stronger repulsion pushes the first peak to a larger distance which may have resulted in an overlap with a second peak, leading to a fairly flat top. The difference in electric charge on the phosphoryl group can result in a substantial difference in PCFs because the electrostatic interaction is orders of magnitude stronger than the van der Waals dispersion force. In addition, the more complex TBP molecule (compared to, say, a small dipolar water molecule), i.e., with nonpolar tails, is much less effective in screening the electrostatic interaction.

3.4.3. P−O2 Pair Correlation Function (Figure 5)

- DFT charge. There is a main peak at around 5.3 Å, a weak peak around 7.4 Å, and a broad peak around 12.5 Å. The peak at 5.3 Å may correspond to the approach of the O2 atom to the P atom in the space between the P−O2 and P−OS bonds, so it is closer than the sum of the O2−O2 peak position (4.9 Å) and the P−O2 bond distance (1.48 Å).
- MNDO charge. There is a shoulder starting around 5.5 Å, a relatively broad peak at 8.0 Å, and a weak peak around 13 Å. Again, the stronger repulsion between the O2−O2 and P−P pairs of two TBP molecules seems to have prevented the appearance of the first peak around 5.5 Å, resulting in a broad peak at 8.0 Å.

3.4.4. O2−OS Pair Correlation Function (Figure 6). This pair correlation is calculated including contributions from all three OS atom types of the TBP molecule without making a distinction among them.

- DFT charge. Three peaks are located at positions 4.6, 6.8, and 12.3 Å. There is also a shoulder starting around 9.0 Å.
- MNDO charge. There appears to be a shoulder starting around 4.7 Å and a broad peak around 9.0 Å. Such a broad peak could indicate an overlap of potentially more than

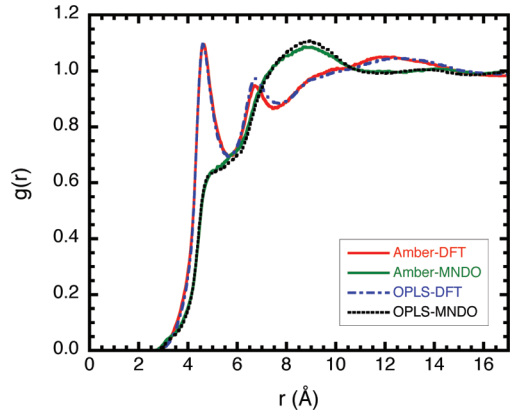

Figure 6. Pair correlation for O2−OS; line types as in Figure 3.

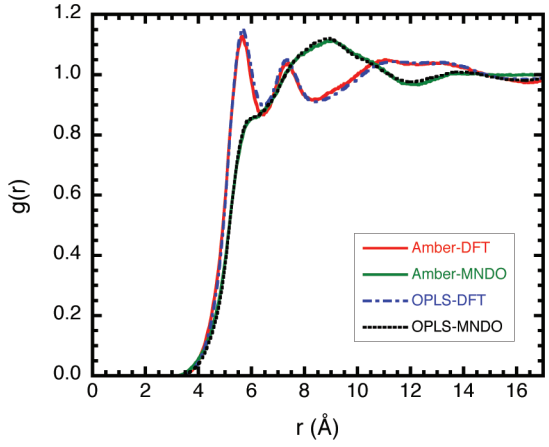

Figure 7. Pair correlation for P−OS; line types as in Figure 3.

one peak.The DFT charge allows the atoms to closely approach each other; thus, the corresponding PCFs exhibit more pronounced features. The first peak of the DFT PCFs turns into a shoulder in the MNDO PCFs, and the second peak together with the shoulder at 9.0 Å turns into a broad peak for the MNDO PCFs.

3.4.5. P−OS Pair Correlation Function (Figure 7). This pair correlation function is calculated in the same way as the O2−OS pair correlation function; thus, all three OS atom types are equivalent.

- DFT charge. There exists two well-defined peaks at positions 5.7 and 7.4 Å and a broad bump between 11 and 14 Å, suggesting the overlap of two peaks.
- MNDO charge. A shoulder at about 5.8 Å and a peak around 9.0 Å are present.Comparison of the DFT and MNDO charged PCFs shows that the shoulder position of the MNDO PCFs is fairly close to the first peak position for the DFT PCFs, suggesting a suppressed peak due to the repulsion between two phosphoryl groups of TBP with MNDO charge. Consequently, the second peak of the DFT PCFs is pushed out to result in the MNDO peak at 9.0 Å.

3.4.6. O2−C Pair Correlation Function (Figure 8). This pair correlation function type includes contribution from all carbon atoms without taking into consideration their position in the TBP molecule structure.

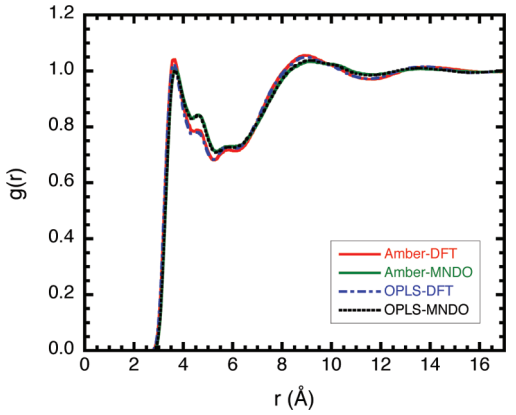

Figure 8. Pair correlation for O2−C; line types as in Figure 3.

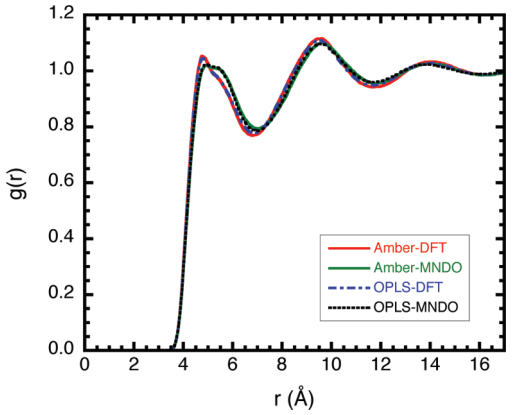

Figure 9. Pair correlation for P−C; line types as in Figure 3.

- DFT charge. There exists a peak at 3.6 Å, followed by two weak peaks and a broad peak around 9.0 Å.
- MNDO charge. Essentially the same features as for the DFT charge PCFs are found.All PCFs are similar except for some minor differences in peak heights. The reason for this result is that the carbon atoms are less charged than the atoms of the phosphoryl group. Taken together with the hydrogen, the methyl and methylene groups are close to neutral, so the difference due to the charge effect is much smaller. In addition, the carbon atoms near the terminals of the butyl tails are likely to be more accessible and the charge differences for them are much smaller than between the interior C_a carbon type in the two force field models.

3.4.7. P−C Pair Correlation Function (Figure 9). This PCF is calculated in the same way as the O2−C pair correlation function.

- DFT charge. Three peaks are located at positions 4.8, 9.5, and 13.9 Å. There appears to be a weak shoulder after the first peak.
- MNDO charge. Here, peak positions are very similar: 5.0, 9.6, and 14.0 Å. The shoulder in the PCF for the DFT charge has merged into the first peak to result in a broad first peak. For the same reason as the O2−C PCFs, the P−C PCFs for the two charge sets are very similar. When compared to the O2−C PCFs, the locations of the first peaks occur at a distance larger by about 1.21−1.35 Å, which is close to the P−O2 equilibrium bond distance 1.48 Å.

dx.doi.org/10.1021/jp207089e |*J. Phys. Chem. B* 2012, 116, 305–313

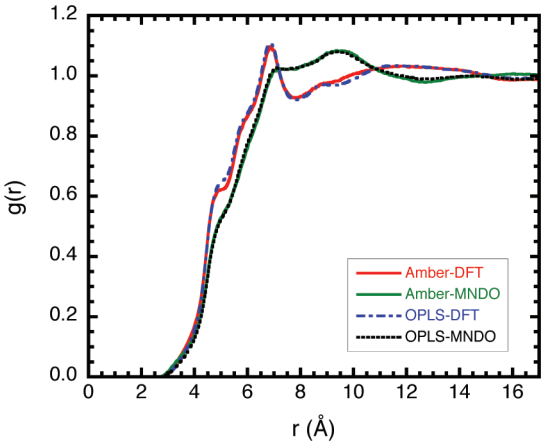

Figure 10. Pair correlation for OS−OS; line types as in Figure 3.

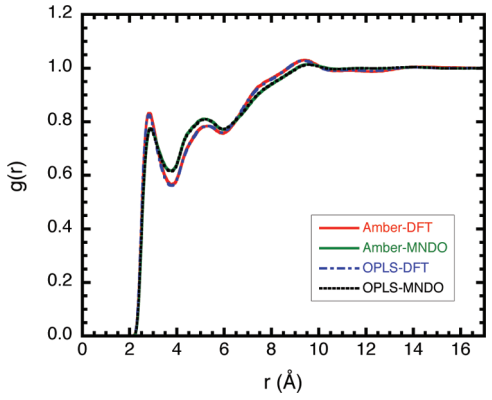

Figure 11. Pair correlation for O2−H; line types as in Figure 3.

3.4.8. OS−OS Pair Correlation (Figure 10). Contributions from all three OS atom types (i.e., all nine pairs) were accumulated; i.e., a distinction between these atom types was not made.

- DFT charge. A shoulder is found at about 4.8 Å, a peak, at 6.9 Å, a weak shoulder, at about 8.7 Å, and a broad peak, at about 11.5 Å.
- MNDO charge. A weak shoulder starts at about 4.8 Å, a second shoulder around 7.0 Å, and a peak at around 9.5 Å. The shoulder (or peak) positions at 4.8 and 7.0 Å for the two sets of charges roughly match each other. The presence of several shoulders and weak peaks is related to the OS atoms' positions in the TBP molecule, which are less accessible.

3.4.9. O2−H Pair Correlation Function (Figure 11). All hydrogen atoms are treated as equal; i.e., no distinction is made between the hydrogen atoms on different carbons.

- DFT charge. Three peaks are at the positions 2.9, 5.4, and 9.4 Å. A shoulder is at about 7.5 Å.
- MNDO charge. Two peaks are at 2.8 and 5.4 Å, and the third peak at 9.5 Å is relatively weak and broad. There is a faint shoulder around 7.5 Å.The pair correlation functions are essentially the same as expected from the earlier discussion for the O2−C case.

3.4.10. Effect of Scaled Charges on PCFs. When the partial atomic charge in the force field models is reduced, to approximate the experimental value of the electric dipole moment (section 3.1), only the PCFs for atoms of the phosphoryl headgroup are significantly affected. The PCFs involving atoms of the butyl tail group are essentially unchanged.

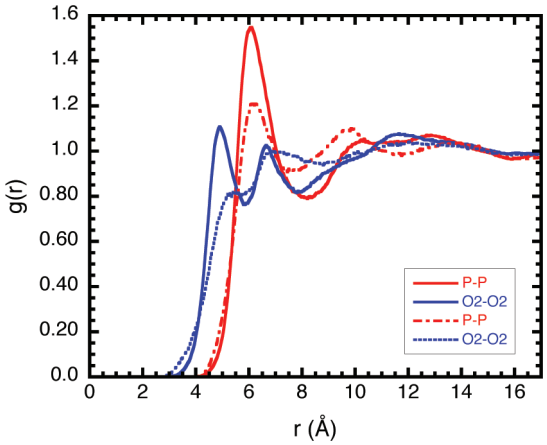

Figure 12. Comparison of PCFs for the P−P and O2−O2 atom type pairs between DFT unscaled atomic partial charges: P−P (solid red line); O2−O2 (solid blue line), and DFT scaled charges (scaling factor 0.70): P−P (long dashed-short dashed red line); O2−O2 (dotted blue line).

Charge reduction tends to allow for atom pairs to closely approach each other. It also tends to reduce the height of the first peak of the PCFs. This is because at close distances the head groups are generally repulsive to each other; hence, decreasing the charge decreases the repulsion (Figure 12).

The first PCF peak is determined by the van der Waals exclusion at short distance and the mean attraction between the atom pairs in the liquid environment. Decreasing the charge weakens the mean attraction at the equilibrium distance between the atom pair so that the first peak height is reduced. All other PCFs comparing the effect of scaled charges are made available as Supporting Information (section 4).

4. SUMMARY

The performance of four sets of force field models in predicting some TBP thermophysical properties in the liquid state has been examined. The results show that the AMBER intramolecular force field model with both the MNDO and the DFT determined charge for an isolated TBP molecule overpredicts the experimental electric dipole moment in the liquid phase. Therefore, we carried out calculations using scaled charge sets to approximate the average experimental value of the dipole moment. This leads to a reduction of charge by about 40% for the MNDO charge and about 30% for the DFT charge.

The agreement between the predicted and experimental mass density is improved when using the scaled charges. Using the unscaled charge sets, the force fields predict mass density to within 2.30% for OPLS-MNDO, 2.78% for OPLS-DFT, 1.06% for AMBER-MNDO, and 1.33% for AMBER-DFT. Using the scaled charges that approximate the experimental dipole moment, the predicted mass density is within 0.47, 0.98, and 0.45%, respectively. Thus, very good agreement is achieved for the mass density and the associated dipole moment.

All pair correlation functions involving the atoms in the phosphoryl group were computed. Since the LJ parameters of the phosphoryl group were unchanged between the AMBER and OPLS parameter sets, the calculated pair correlation functions

differed mainly in the charge sets used, that is, either MNDO or DFT. The main difference is that, for the DFT charge based models, the atoms of the phosphoryl group are able to approach each other more closely, so that the resulting PCFs exhibit more structure. For the MNDO charge based models, the atoms of the phosphoryl group are, on average, more separated, so that the resulting PCFs are more diffuse in structure at short distances. In general, the PCFs differ only for atoms of the phosphoryl group while very little difference is observed for PCFs involving the atoms of the butyl tails; the same is true when the charge is scaled.

On the basis of the properties studied, all force field models reasonably predict mass density. The scaled charge models predict accurately both the dipole moment and the improved mass density to within 1%. All force fields underpredict the self-diffusion coefficient. The OPLS-based fields predict a self-diffusion coefficient that is in relatively better agreement with experiment than the AMBER-based force fields. In this work, we have not tried to optimize the van der Waals parameters of the phosphoryl headgroup of the TBP. We speculate that fine-tuning these parameters may improve the fidelity of the prediction of the self-diffusion coefficient and other transport properties.

■ ASSOCIATED CONTENT

Supporting Information. Additional plot of pressure variation with mass density for scaled charges. Various pair correlation functions with unscaled and scaled charges. This material is available free of charge via the Internet at http://pubs.acs.org.

■ AUTHOR INFORMATION

Corresponding Author

*E-mail: scui@utk.edu; dealmeidav@ornl.gov.

■ ACKNOWLEDGMENT

This work was supported by the US Department of Energy, Office of Nuclear Energy under the Nuclear Energy University Program (DOE-NEUP), contract number: DE-AC07-051D14517. Computing resources used at the Center for Advanced Modeling and Simulation at the Idaho National Laboratory through a collaboration with the Nuclear Energy Advanced Modeling and Simulation program of the Nuclear Energy Office of DOE are greatly appreciated. The Oak Ridge National Laboratory is managed by UT-Battelle, LLC for the DOE under contract No. DE-AC05-00OR22725.

■ REFERENCES

(1) Chiarizia, R.; Jensen, M. P.; Borkowski, M.; Ferraro, J. R.; Thiyagarajan, P.; Littrell, K. C. *Solvent Extr. Ion Exch.* **2003**, *21*, 1–27.

(2) Chiarizia, R.; Nash, K. L.; Jensen, M. P.; Thiyagarajan, P.; Littrell, K. C. *Langmuir* **2003**, *19*, 9592–9599.

(3) Zilberman, B. Y.; Fedorov, Y. S.; Kopyrin, A. A.; Arkhipov, S. A.; Blazheva, I. V.; Glekov, R. G. *Radiochemistry* **2001**, *43*, 172–174.

(4) Moyer, B. A. *Solvent extraction: fundamentals to industrial applications*; Proceedings of ISEC 2008 International Solvent Extraction Conference v. 1−2; Canadian Institute of Mining, Metallurgy and Petroleum, 2008.

(5) Shukla, J. P.; Misra, S. K. *Indian J. Chem., Sect. A: Inorg., Bio-inorg., Phys., Theor. Anal. Chem.* **1995**, *34*, 778–786.

(6) Plaue, J.; Gelis, A.; Czerwinski, K.; Thiyagarajan, P.; Chiarizia, R. *Solvent Extr. Ion Exch.* **2006**, *24*, 283–298.

(7) Chiarizia, R.; Jensen, M. P.; Rickert, P. G.; Kolarik, Z.; Borkowski, M.; Thiyagarajan, P. *Langumir* **2004**, *20*, 10798–10808.

(8) Nave, S.; Mandin, C.; Martinet, L.; Berthon, L.; Testard, F.; Madic, C.; Zemb, T. *Phys. Chem. Chem. Phys.* **2004**, *6*, 799–808.

(9) Cui, S.; de Almeida, V. F.; Khomami, B. In *Solvent Extraction: Fundamentals to Industrial Applications*; Moyer, B. A., Ed.; Canadian Institute of Mining, Metallurgy and Petroleum: Montreal, Quebec, Canada; 2008; pp 1069−1075.

(10) Ye, X.; Cui, S.; de Almeida, V. F.; Khomami, B. *J. Phys. Chem. B* **2009**, *113*, 9852–9862.

(11) Ye, X.; Smith, R. B.; Cui, S.; de Almeida, V. F.; Khomami, B. *Solvent Extr. Ion Exch.* **2010**, *28*, 1–18.

(12) Ye, X.; Cui, S.; de Almeida, V. F.; Hay, B. P.; Khomami, B. *Phys. Chem. Chem. Phys.* **2010**, *12*, 15406–15409.

(13) Wallace, W. S., James, D. N., Eds. *The Science and Technology of Tributyl Phosphate*; CRC Press: Boca Raton, FL, 1984; Vol. 1−4.

(14) Tian, Q. L.; Liu, H. Z. *J. Chem. Eng. Data* **2007**, *52*, 892–897.

(15) Beudaert, P.; Lamare, V.; Dozol, J. F.; Troxler, L.; Wipff, G. *Solvent Extr. Ion Exch.* **1998**, *16*, 597–618.

(16) Beudaert, P.; Lamare, V.; Dozol, J. F.; Troxler, L.; Wipff, G. *J. Chem. Soc., Perkin Trans. 2* **1999**, *11*, 2515–2523.

(17) Schurhammer, R.; Wipff, G. *J. Phys. Chem. A* **2005**, *109*, 5208–5216.

(18) Ponder, J. TINKER - Software Tools for Molecular Design. http://dasher.wustl.edu/tinker/, 2011; Amber99 parameter file at http://dasher.wustl.edu/tinker/distribution/params/amber99.prm.

(19) Wang, J.; Cieplak, P.; Kollman, P. *J. Comput. Chem.* **2000**, *21*, 1049–1074.

(20) Cornell, W. D.; Cieplak, P.; Bayly, C. I.; Gould, I. R.; Merz, K. M.; Ferguson, D.; Spellmeyer, D.; Fox, T.; Caldwell, J. W.; Kollman, P. *J. Am. Chem. Soc.* **1995**, *117*, 5179–5197.

(21) Dewar, M. J. S.; Thiel, W. *J. Am. Chem. Soc.* **1977**, *99*, 4899–4907.

(22) Bayly, C. I.; Cieplak, P.; Cornell, W. D.; Kollman, P. A. *J. Phys. Chem.* **1993**, *97*, 10269–10280.

(23) Valiev, M.; Bylaska, E. J.; Govind, N.; Kowalski, K.; Straatsma, T. P.; Van Dam, H. J. J.; Wang, D.; Nieplocha, J.; Apra, E.; Windus, T. L.; de Jong, W. *Comput. Phys. Commun.* **2010**, *181*, 1477–1489.

(24) Becke, A. D. *J. Chem. Phys.* **1993**, *98*, 5648–5652.

(25) Lee, C. T.; Yang, W. T.; Parr, R. G. *Phys. Rev. B* **1988**, *37*, 785–789.

(26) Deleeuw, S. W.; Perram, J. W.; Smith, E. R. *Proc. R. Soc. London, Ser. A* **1980**, *373*, 27–56.

(27) Allen, M. P.; Tildesley, D. J. *Computer Simulation of Liquids*; Clarendon Press: Oxford, Great Britain, 1987.

(28) Jorgensen, W.; Maxwell, D.; TiradoRives, J. *J. Am. Chem. Soc.* **1996**, *118*, 11225–11236.

(29) Alejandre, J.; Tildesley, D. J.; Chapela, G. A. *J. Chem. Phys.* **1995**, *102*, 4574–4583.

(30) Tuckerman, M.; Berne, B. J.; Martyna, G. J. *J. Chem. Phys.* **1992**, *97*, 1990–2001.

(31) Nosé, S. *Mol. Phys.* **1984**, *52*, 255–268.

(32) Nosé, S. *J. Chem. Phys.* **1984**, *81*, 511–519.

(33) Petkovic, D. M.; Kezele, B. A.; Rajic, D. R. *J. Phys. Chem.* **1973**, *77*, 922–924.

(34) Estok, G. K.; Wendlandt, W. W. *J. Am. Chem. Soc.* **1955**, *77*, 4767–4769.

(35) Johnson, W. F.; Dillon, R. L. *Physical Properties of Tributylphosphate-Diluent*; Report HW-29086, 1953.

(36) Firlej, L.; Kuchta, B.; Roth, M. W.; Wexler, C. *J. Mol. Model.* **2011**, *17*, 811–816.